Int J Adv Struct Eng (2016) 8:193–212
DOI 10.1007/s40091-016-0123-z

ORIGINAL RESEARCH

Analysis, prediction, and case studies of early-age cracking in bridge decks

Adel ElSafty[1] · Matthew K. Graeff[2] · Georges El-Gharib[3] · Ahmed Abdel-Mohti[4] · N. Mike Jackson[5]

Received: 25 April 2016 / Accepted: 4 May 2016 / Published online: 14 May 2016

Abstract Early-age cracking can adversely affect strength, serviceability, and durability of concrete bridge decks. Early age is defined as the period after final setting, during which concrete properties change rapidly. Many factors can cause early-age bridge deck cracking including temperature change, hydration, plastic shrinkage, autogenous shrinkage, and drying shrinkage. The cracking may also increase the effect of freeze and thaw cycles and may lead to corrosion of reinforcement. This research paper presents an analysis of causes and factors affecting early-age cracking. It also provides a tool developed to predict the likelihood and initiation of early-age cracking of concrete bridge decks. Understanding the concrete properties is essential so that the developed tool can accurately model the mechanisms contributing to the cracking of concrete bridge decks. The user interface of the implemented computer Excel program enables the user to input the properties of the concrete being monitored. The research study and the developed spreadsheet were used to comprehensively investigate the issue of concrete deck cracking. The spreadsheet is designed to be a user-friendly calculation tool for concrete mixture proportioning, temperature prediction, thermal analysis, and tensile cracking prediction. The study also provides review and makes recommendations on the deck cracking based mainly on the Florida Department of Transportation specifications and Structures Design Guidelines, and Bridge Design Manuals of other states. The results were also compared with that of other commercially available software programs that predict early-age cracking in concrete slabs, concrete pavement, and reinforced concrete bridge decks. The outcome of this study can identify a set of recommendations to limit the deck cracking problem and maintain a longer service life of bridges.

Keywords Cracking · Early-age · Bridge deck · Temperature · Shrinkage

✉ Ahmed Abdel-Mohti
a-abdel-mohti@onu.edu

[1] Civil Engineering Department, University of North Florida, Jacksonville, FL, USA

[2] Segars Engineering , 1200 Five Springs Rd., Charlottesville, VA, USA

[3] Johnson, Mirmiran & Thompson, Inc., Lake Mary, FL, USA

[4] Civil Engineering Department, Ohio Northern University, Ada, OH, USA

[5] Department of Civil Engineering and Construction Management, Georgia Southern University, Statesboro, GA, USA

Introduction

Transverse cracking has been observed in many bridge decks in Florida and other states (e.g., Wan et al. 2010). Transverse deck cracking is more likely to occur in early ages. The ACI Committee 231, Properties of Concrete at Early Ages, identified "early age" as the period after final setting (ACI 231 2010). During this period, concrete properties change rapidly. Early-age volume changes are induced by temperature change, hydration, and drying shrinkage. This volume change can lead to early-age cracking due to restraint of volume changes associated with thermal deformation, shrinkage due to hydration reactions, and shrinkage due to drying. Such cracking can adversely affect strength, serviceability, and durability of bridge decks. Also, the development of deck cracking increases the effect of freeze and thaw cycles which may lead to spalling of concrete, and thus, resulting in corrosion of

steel reinforcement. Transverse deck cracking may also increase carbonation and chloride penetration leading to accelerated steel reinforcement corrosion. Also, a possible damage to underlying components may take place, and the bridge may experience premature deterioration. Therefore, transverse deck cracks affect bridges causing loss of stiffness, and eventually, loss of function, undesirable esthetic condition, reduction of service life of structures, and increase in maintenance costs.

Several studies investigated the issue of deck cracking (Manafpour et al. 2015; Wright et al. 2014; Maggenti et al. 2013; Peyton et al. 2012; Darwin et al. 2012; Slatnick et al. 2011; McLeod et al. 2009; Wan et al. 2010; French et al. 1999; Babaei and purvis 1996; Krauss and Rogalla 1996; La Fraugh and Perenchio 1989; Babaei and Hawkins 1987; PCA 1970). Numerous factors can affect transverse deck cracking in highway bridges including time-dependent material properties, restraints, casting sequence, formwork, and environmental factors. The aforementioned studies determined that span continuity, concrete strength, and girder type are the most important design factors influencing transverse cracking. The design factors most related to transverse cracking are longitudinal restraint, deck thickness, and top transverse bar size. Material properties such as cement content, cement composition, early-age elastic modulus, creep, aggregate type and quantity, heat of hydration, air content, and drying shrinkage also influence deck cracking. Schmitt and Darwin (1999) conducted a study considering various site conditions factors such as average air temperature, low air temperature, high air temperature, daily temperature range, relative humidity, average wind velocity, and evaporation. To investigate the concrete cracking in new bridge decks and overlays, Wan et al. (2010) completed a Wisconsin Department of Transportation (DOT) project indicating that the rapid development of compressive strength and modulus of elasticity of concrete may lead to significant shrinkage and tensile stresses in the deck. Table 1 shows a sample of departments of transportation projects addressing concrete bridge deck cracking.

Research objectives

The objective of this research study is to investigate the early-age cracking and its mitigation. In this study, a tool was developed to facilitate predicting the early-age cracking in bridge decks. It helps in predicting cracks in both under-construction and future bridge decks. Two case studies were investigated to examine the issue of cracking and to compare the outcome of the developed tool to that of an available software program "HIPERPAV". After verification, the tool was used to check the cracking tendency in newer bridges with different material properties. Also, field investigation was conducted to observe deck cracking in existing bridge decks and monitor the development of transverse cracks in new bridge under construction. In general, the ultimate goal of this research study is to provide a comprehensive insight of the issue of early-age cracking in bridge deck and to provide recommendations to limit the problem.

Field investigation

Field investigation was conducted in this study to observe the pattern and locations of cracks developed in several existing bridge decks (Fig. 1a–h). A number of bridges were inspected, assessed, and repaired with sealers including Florida bridges in Fort Lauderdale, Jacksonville, and Pensacola. Investigation was also performed to observe the crack development in a new bridge "US 1 Bridge" under construction. Most of the observed cracks have an average width of 0.02 inch, and they are spaced about 3–4 ft apart. A number of tests were performed in a previous study to evaluate and treat existing cracks (ElSafty and Jackson 2012; ElSafty and Abdel-Mohti 2013; El Safty et al. 2013). The results were in agreement with Manafpour et al. (2015) in which it was observed that initial observation of early-age deck cracks was within the first 2 months after concrete placement and was more pronounced during summer time.

Table 1 DOTs concrete bridge deck cracking

Department of transportation	Year	Title
PennDOT	2015	Bridge deck cracking: effects on in-service performance, prevention, and remediation
FDOT	2012	Sealing of cracks on florida bridge decks with steel girders
NYDOT	2011	Tool for analysis of earlyage transverse cracking of composite bridge decks
WisconsinDOT	2010	Concrete cracking in new bridge decks and overlays
ALDOT	2010	Evaluation of cracking of the US 331 bridge deck
CDOT	2003	Assessment of the cracking problem in newly constructed bridge decks in Colorado
MDOT	1998	Transverse cracking in bridge decks: field study

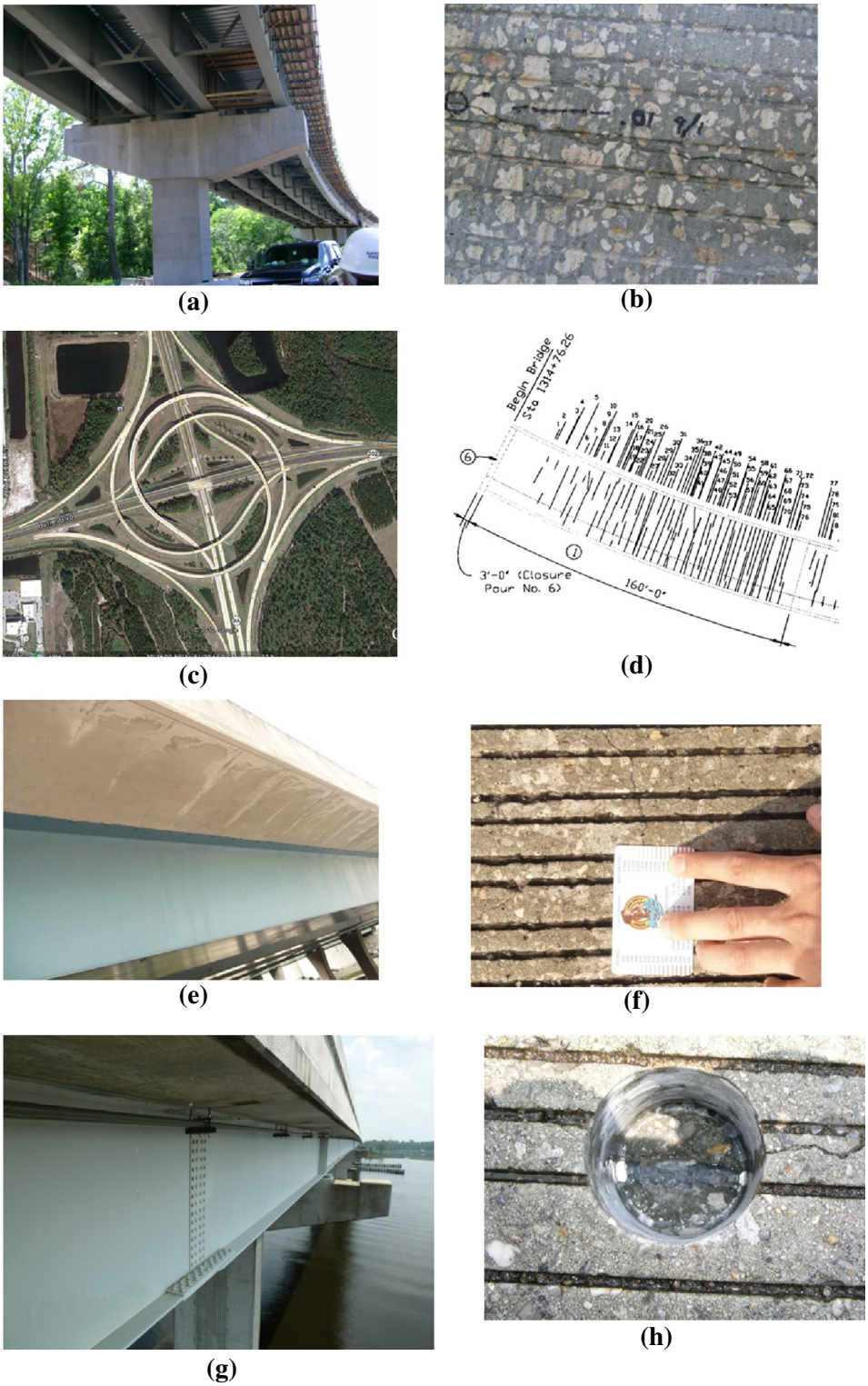

Fig. 1 Bridge deck cracking. **a** US 1 bridge (Jacksonville, Florida), **b** Close up view of deck crack, **c** JTB bridge (Jacksonville, Florida), **d** Deck crack pattern, **e** Fort Lauderdale bridge (Florida), **f** Close up view of the deck crack, **g** Blackwater River Bridge (Milton-Pensacola, Florida), **h** Core sampling showing crack development over the transverse reinforcement

Development of a tool to predict deck cracking

Understanding thoroughly the concrete properties is vital to accurately model the mechanisms contributing to the cracking of concrete decks. The deck cracking Excel spreadsheet tool was developed in this study to facilitate conducting a number of case studies and to predict the potential transverse deck cracking of bridges. The user interface of the developed Excel program enables the user to input the properties of the concrete being monitored. The

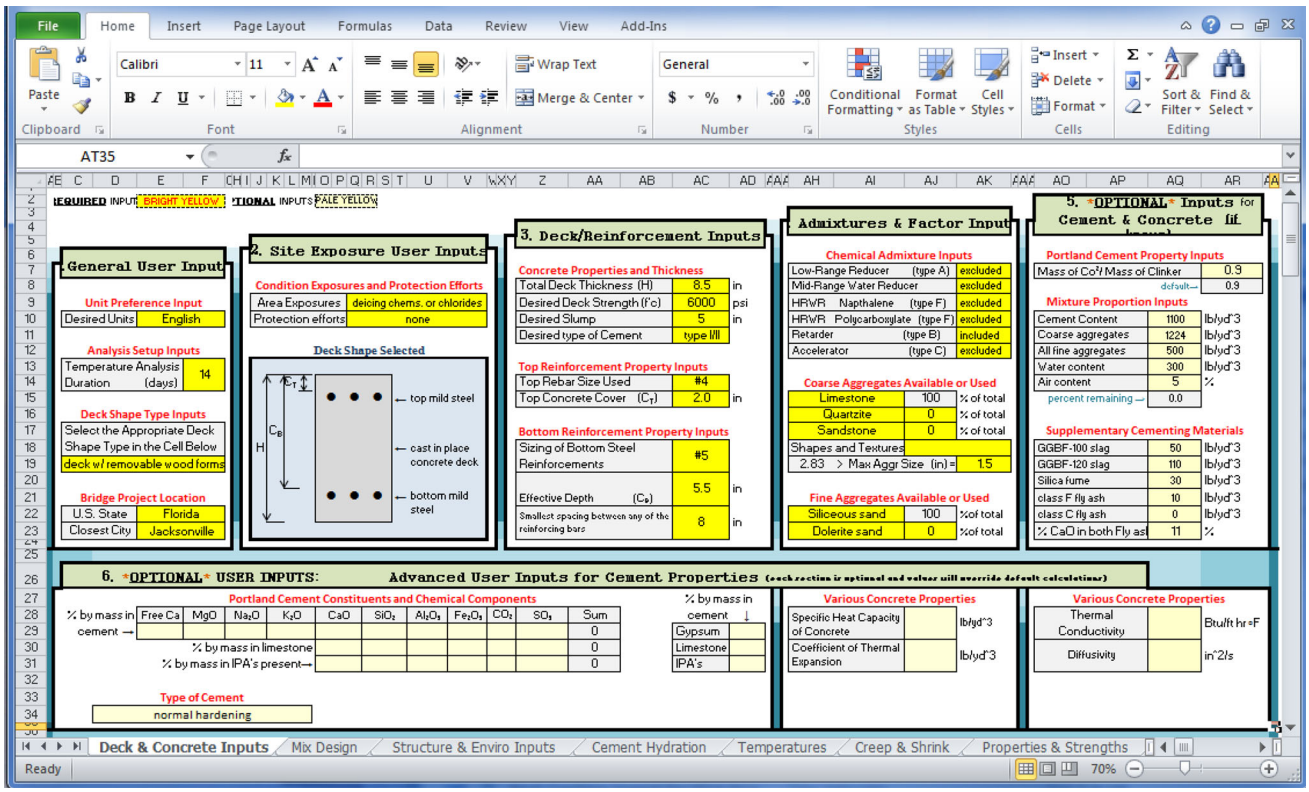

Fig. 2 Deck and concrete inputs

spreadsheet is designed to be a user-friendly calculation tool for concrete mixture proportioning, temperature prediction, thermal analysis, and tensile cracking prediction. It is designed specifically for concrete bridge decks. It also addresses different types of construction approaches including a deck with a stay-in-place galvanized metal pan, a deck with removable forms, and a deck on a precast panel. The user should address the fundamental principles and mechanics of concrete hardening to obtain accurate temperatures, thermal stresses, and cracking risk calculations. Also, it is advisable to follow available recommendations to limit concrete deck cracking such as Manafpour et al. (2015). The aspects of concrete hardening addressed in the spreadsheet is subdivided into multiple sections; the first being concrete mixture proportioning, followed by temperature prediction, thermal stress analysis, and finally tensile cracking predictions.

The spreadsheet has multiple tabs that show the logical steps that a designer would follow during a design process. The tabs include Deck and Concrete Inputs, Mix Design, Structural and Environmental Inputs, Cement Hydration, Temperature Analysis, Properties and Strengths, Creep and Shrinkage Stresses, and Result Summary. Each tab may contain various required user inputs, optional user inputs, default values, or calculated values. Each of the cells is color coded. Examples of a user input tab is shown in Fig. 2.

Recommendations for design inputs

A designer would need to determine all the necessary design inputs to achieve an accurate assessment of the likelihood of reinforced concrete deck cracking. Figure 2 summarizes all the necessary deck and concrete inputs. The Deck and Concrete Inputs worksheet values are in accordance with the current engineering practices. Since the Materials Research Report which is titled Sealing of Cracks on Florida Bridge Decks with Steel Girders, was created for FDOT, it is recommended to verify the input values against the most recent FDOT Standard Specifications for Road and Bridge Construction (FDOT Specs) and the FDOT Structures Manual Volume 1 Structures Design Guidelines (FDOT SDG). Other Departments of Transportation Bridge Design Manuals were also used (i.e., Ohio DOT, Pennsylvania DOT, Indiana DOT).

The summary below is a list of recommendations for the Deck/Reinforcement Inputs:

1. Total deck thickness (H): The FDOT SDG requires that cast-in-place deck thickness shall be 8.0 inches for short bridges and 8.5 inches for long bridges (SDG 4.2.2). The determining length is the length of the bridge structure measured along the profile grade line (PGL) from front face of backwall at Begin Bridge to

Table 2 Range of user override water adjustment factors

Factor	Adjustment ranges (negative is reduction)			
Normal range water reducer (ASTM type A)	0	%	−10	%
Mid-range water reducer	−8	%	−15	%
High range water reducer (ASTM type F)	−12	%	−30	%
Air entrainment effect	5	lbs/% air needed for desired %		
Aggregate shape and texture	−20	lbs	−45	lbs
Aggregate gradation	10	%	−10	%
Supplementary mineral admixtures	15	%	−10	%
Other unspecified factors	10	%	−10	%

front face of backwall at End Bridge of the structure. Short bridges and long bridges are defined in Section 4.2.1 of the FDOT SDG as follows:

(a) Short bridges: bridge structures less than or equal to 100 ft in PGL length.
(b) Long bridges: bridge structures more than 100 ft in PGL length.

The Ohio DOT (ODOT) Bridge Design Manual (BDM) requires calculating a minimum reinforced concrete deck thickness using the following equation (BDM 302.2.1):

$$T_{\min}(\text{inches}) = (S + 17)(12)/36 \geq 8.5 \text{ inches} \quad (1)$$

where S is the effective span length in feet determined in accordance with AASHTO LRFD 9.7.3.2 (AASHTO 2007). The minimum deck thickness includes a 1 inch wearing surface.

ODOT also offers a Concrete Deck Design Aid table that shows the deck thickness based on the effective span length. The deck thicknesses in this table range from 8.5 to 10.5 inches. ODOT does not allow the use of precast deck panels, since they have shown cracking problems at the joints between the panels, and there are questions on the transfer of stresses in the finished deck sections. The Pennsylvania DOT (PennDOT) Design Manual Part 4 Structures (DM-4) recommends a minimum reinforced concrete deck thickness of 8.0 inches (Part B, 9.7.1.1) which includes a 0.5 inch wearing surface. This is also true for both reinforced and prestressed precast concrete deck panels (Part B, 9.7.5.1). The Indiana DOT (INDOT) Design Manual Chapter 404 (Ch404) Bridge Deck requires the reinforced deck depth to be a minimum of 8.0 inches that includes 0.5 inch of sacrificial wearing surface (404-2.01.2). The AASHTO LRFD Bridge Design Specifications (LRFD) requires that the minimum thickness of a reinforced concrete deck should not be less than 7.0 inches (LRFD 9.7.1.1), if approved by the owner. This minimum thickness does not include any provision for grinding, grooving, and sacrificial surface. For precast decks on girders, the minimum thickness of a reinforced concrete deck and prestressed concrete deck should not be less than 7.0 inches (LRFD 9.7.5.1). Based on the information mentioned above, it is recommended that a range of 7.0–11.0 inches with 0.5 inch increments be used in the total deck thickness.

2. Desired deck strength ($f'c$): The FDOT SDG Table 1.4.3-1 requires that cast-in-place concrete deck shall have the following structural class:
   (a) Class II (bridge deck) for slightly aggressive environment.
   (b) Class IV for moderately and extremely aggressive environment.

The environmental classification is based on Section 1.3 of the SDG. Concrete classes are defined in Section 346, Portland cement concrete, of the FDOT Specifications. The concrete specified minimum strength at 28 days is shown in the list below:

(a) For class II concrete (bridge deck): 4500 psi.
(b) For class IV concrete: 5500 psi.

The ODOT BDM requires the deck concrete to be Class S or Class HP (BDM 302.1.2.2) with a minimum 28-day compressive strength of 4500 psi (BDM 302.1.1). The PennDOT DM4 requires the deck concrete to be Class AAA with a minimum 28-day compressive strength of 4000 psi (DM4 Part B, 5.4.2.1). The INDOT Ch404 requires the deck concrete to be Class C (404-2.01.6) with a minimum 28-day compressive strength of 4000 psi (404-2.01.7). Based on the information mentioned above, this research considered a range of 3000–5500 psi.

3. Desired Slump: The FDOT Specifications Section 346-3.1. Table 2 shows a target slump value of 3 inches for both Class II (Bridge Deck) and Class IV concrete with a ±1.5 inch tolerance (Specs 346-6.4). ACI 301 requires a slump of 4 inches at the point of delivery (ACI 301-4.2.2.2) with a tolerance of ±1 inch (ACI 301 2010). Based on the information mentioned above, the research considered a range of 1–7 inches in the desired slump.
4. Top concrete cover: The FDOT SDG requires that cast-in-place decks shall have the following top concrete cover (Table 1.4.2-1):

(a) Short bridges: 2 inches.
(b) Long bridges: 2.5 inches.

The ODOT BDM requires a 2.5 inches minimum cover for the concrete deck top surface (BDM 301.5.7). The PennDOT DM4 requires a 2.5 inches minimum cover for the concrete deck top surface (DM4 Part B, 5.12.3). The INDOT Ch404 requires a 2.5 inches minimum cover for the concrete deck top surface (404-2.01.3). Based on the information mentioned above, this research considered a range of 2–3.0 inches to be used in the top concrete cover.

5. Effective depth: The FDOT SDG requires that cast-in-place decks shall have a bottom reinforcement concrete cover of 2.0 inches (Table 1.4.2-1). The ODOT BDM requires a 1.5 inch minimum cover for the concrete deck bottom surface (BDM 301.5.7). The PennDOT DM4 requires a 1.0 inch minimum cover for the concrete deck bottom surface (DM4 Part B, 5.12.3). The INDOT Ch404 requires a 1.0 inch minimum cover for the concrete deck bottom surface (404-2.01.3). The effective depth is a function of the deck thickness and the reinforcement cover to the bottom surface of deck. Assuming that the deck thickness varies from 7 to 11 inches and the minimum cover to the bottom surface is 1.0 inch, this research considered a range of 6–10.0 inches to be used in the effective depth.

Mix design worksheet

The primary source commonly used for the mixture proportioning calculations is the ACI 211.1-91 document "Standard Practice for Selecting Proportions for Normal, Heavyweight, and Mass Concrete" (ACI 211-91 2009). The basic steps are as follows:

1. Determine the amount of water needed to achieve a given slump for the maximum aggregate size selected by the designer and to make the required adjustments to the water content based on the material properties, chemical admixtures, and entrained air properties.
2. Determine the water to cement ratio needed to achieve a desired strength with the percent of entrained air specified, where the use of supplementary materials is assumed to not affect the water to cement ratio needed to achieve the desired strength.
3. Calculate the coarse aggregate fraction based on the maximum size of aggregate selected and the fine aggregate fineness modulus.
4. Calculate the required amount of fine aggregates to fill the remaining concrete volume since the volume of the cementitious materials, the water content, the coarse aggregate content, and the percentage of air are already included. The fine aggregate weight is then calculated from the volume using the specific gravity of the sands.

In this research, the calculations for concrete mixture proportioning, following the steps presented above, are only performed if the user does not specify a predetermined mixture (Fig. 3). The water content can be adjusted for several factors both with and without a user defined concrete mixture proportion. Table 2 presents typical water adjustment factors.

Structure and environmental inputs

The structure and environmental design inputs are important and will affect the possibility of cracking in bridge decks. The designer will need to determine the properties of both of the deck and girders. Also, information such as type and duration of curing, time of placing concrete, method of curing, temperature at casting, age of concrete at loading, and properties of formwork used, and predication of weather condition after casting are important. Figure 4 shows an example of design inputs.

Temperature prediction

Since early-age properties of concrete change rapidly, the thermal properties of the concrete and its constituents shall be updated at each given time. Some of the time-dependent properties include: thermal conductivity and the specific heat of the concrete. These properties shall be calculated at each time of interest.

Concrete thermal properties

(a) *Thermal Conductivity*: The thermal conductivity is known to be a function of "the moisture content, content and type of aggregate, porosity, density and temperature (Van Breugel 1998)." The concrete thermal conductivity increases with increasing moisture content. Based on the recommendation of Schindler (2002), this research assumes a linear decrease of the thermal conductivity with the degree of hydration from 1.33 times the ultimate thermal conductivity to the ultimate thermal conductivity as shown in Eq. 2:

$$k_c(\alpha) = k_{uc} \cdot (1.33 - 0.33 \cdot \alpha) \quad (2)$$

where k_c is the concrete thermal conductivity (W/m/K), α is the degree of hydration, and k_{uc} is the ultimate hardened concrete thermal conductivity.

(b) *Specific heat capacity*: The specific heat of concrete is also dependent on the mixture proportions, the degree of hydration, moisture levels, and the temperature (Schindler

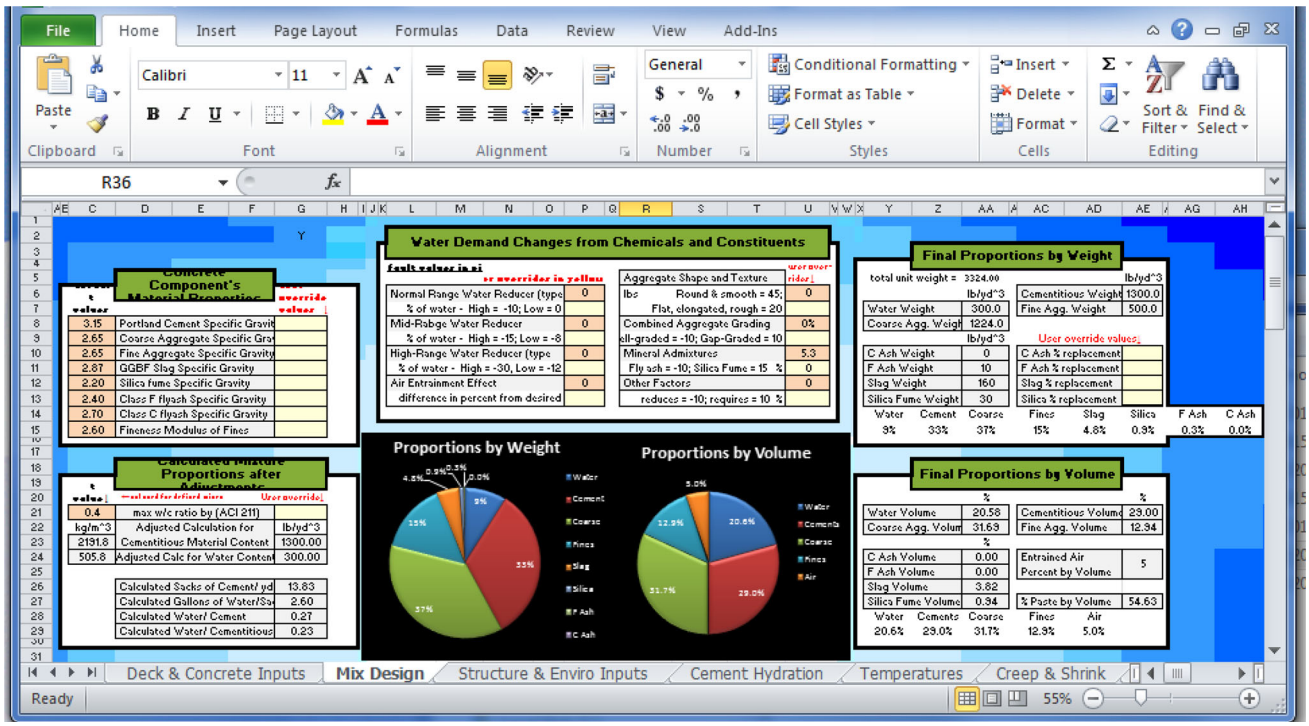

Fig. 3 Mix design

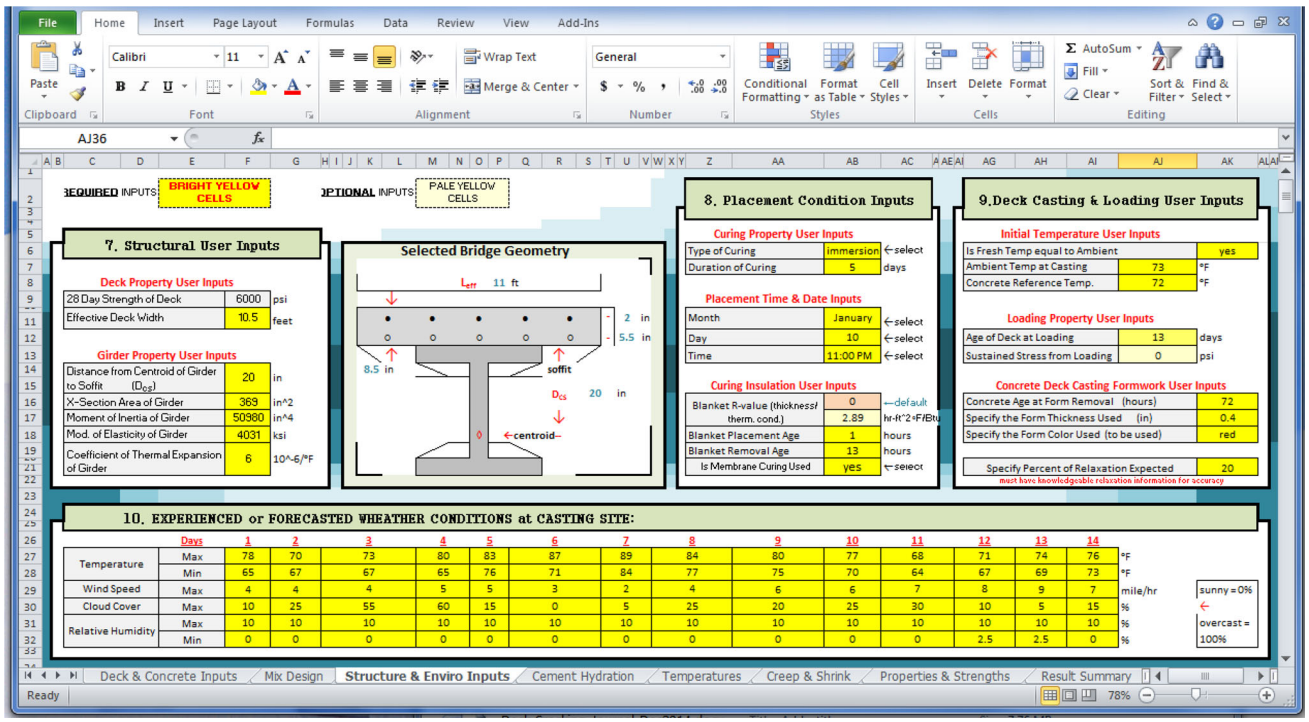

Fig. 4 Example of structural and environmental inputs

2002). A model proposed by Van Breugel accounts for changes in the specific heat based on degree of hydration, mixture proportions, and temperature as shown in Eq. 3.

$$c_{\text{pconc}} = \frac{1}{\rho_{\text{conc}}} \cdot (W_{\text{c}} \cdot \alpha \cdot c_{\text{ref}} + W_{\text{c}} \cdot (1-\alpha) \cdot c_{\text{c}} + W_{\text{a}} \cdot c_{\text{a}} + W_{\text{w}} \cdot c_{\text{w}}) \quad (3)$$

where c_{pconc} is the specific heat of the concrete (J/kg/K), ρ_{conc} is the concrete density (kg/m^3), W_c is the weight of cement (kg/m^3), W_a is the weight of aggregate (kg/m^3), W_w is the weight of water (kg/m^3), c_c is the cement specific heat (J/kg/K), c_a is the aggregate specific heat (J/kg/K), c_w is the water specific heat (J/kg/k), and c_{ref} is an average ultimate specific heat of the cement taken as 840 (J/kg/K).

Concrete heat of hydration

This research accounts for the change in thermal properties of the concrete and its constituents by updating for the change at any given time. For temperature due to hydration, the concrete mix design is first modified using the Bogue calculations according to ASTM C 150. The concrete heat of hydration parameters H_u, τ, β, α_u, and E_a are then calculated based on the concrete mixture proportions and the constituent material properties. The τ, β, and α_u parameters are calculated from Eqs. 4, 5, and 6.

$$\alpha_u = \frac{1.031 \cdot \mathrm{w/cm}}{0.194 + \mathrm{w/cm}} + \exp\left\{\begin{array}{l} -0.885 - 13.7 \cdot p_{C_4AF} \cdot p_{cem} \\ -283 \cdot p_{Na_2O_{eq}} \cdot p_{cem} \\ -9.9 \cdot p_{FA} \cdot p_{FA-CaO} \\ -339 \cdot \mathrm{WRRET} - 95.4 \cdot \mathrm{PCHRWR} \end{array}\right\} \quad (4)$$

$$\tau = \exp \times \left\{\begin{array}{l} 2.68 - 0.386 \cdot p_{C_3S} \cdot p_{cem} + 105 \cdot p_{Na_2O} \cdot p_{cem} + 1.75 \cdot p_{GGBF} \\ -5.33 \cdot p_{FA} \cdot p_{FA-CaO} - 12.6 \cdot \mathrm{ACCL} + 97.3 \cdot \mathrm{WRRET} \end{array}\right\} \quad (5)$$

$$\beta = \exp \times \left\{\begin{array}{l} -0.494 - 3.08 \cdot p_{C_3A} \cdot p_{cem} - 0.864 \cdot p_{GGBF} \\ +96.8 \cdot \mathrm{WRRET} + 39.4 \cdot \mathrm{LRWR} + 23.2 \cdot \mathrm{MRWR} \\ +38.3 \cdot \mathrm{PCHRWR} + 9.07 \cdot \mathrm{NHRWR} \end{array}\right\} \quad (6)$$

Similarly, the parameters of heat and activation energy are also calculated based on the concrete mixture proportions and the constituent material properties as described by Eqs. 7, 8, and 9.

$$\mathrm{Hu} = \left\{\begin{array}{l} H_{cem} \cdot p_{cem} + 461 \cdot p_{GGBF-100} + 550 \cdot p_{GGBF-120} \\ +1800 \cdot p_{FA-CaO} \cdot p_{FA} + 330 \cdot p_{S.F.} \end{array}\right\} \quad (7)$$

$$H_{cem} = \left\{\begin{array}{l} 500 \cdot p_{C_3S} + 260 \cdot p_{C_2S} + 866 \cdot p_{C_3A} + 420 \cdot p_{C_4AF} \\ +624 \cdot p_{SO_3} + 1186 \cdot p_{freeCa} + 850 \cdot p_{MgO} \end{array}\right\} \quad (8)$$

$$E_a = \left\{\begin{array}{l} 41230 + 8330 \cdot [(C_3A + C_4AF) \cdot p_{cem} \cdot \mathrm{Gypsum} \cdot p_{cem}] \\ -3470 \cdot Na_2O_{eq} - 19.8 \cdot \mathrm{Blaine} + 2.96 \cdot p_{FA} \cdot p_{CaO-FA} \\ +162 \cdot p_{GGBFS} - 516 \cdot p_{S.F.} - 30900 \cdot \mathrm{WRRET} - 1450 \cdot \mathrm{ACCL} \end{array}\right\} \quad (9)$$

where p_{C3S} is the percent alite content in the portland cement, p_{C3A} is the percent aluminate in the portland cement, p_{C2S} is the percent belite in the portland cement, p_{C4AF} is the percent ferrite in the portland cement, p_{SO3} is the percent total sulfate in the portland cement, p_{MgO} is the percent MgO in the portland cement, and p_{freeCa} is the percent CaO in the portland cement. Table 3 presents typical dosages of chemical admixtures.

The maturity method used to determine the rate of hydration of the cement is the equivalent age method described in ASTM C 1074 where the equivalent age of the concrete is calculated as described in Eq. 10.

$$t_e = \sum e^{-\frac{E_a}{R}\left(\frac{1}{(T_a+273)} - \frac{1}{(T_r+273)}\right)} \Delta T \quad (10)$$

The degree of hydration is next calculated by use of Eq. 8, and ultimately, the rate of heat generated is calculated using the parameter values from Eqs. 4 through 11 at any given time using Eq. 12 (Schindler and Folliard 2005).

$$\alpha(t_e) = \alpha_u \cdot \exp\left(-\left[\frac{\tau}{t_e}\right]^{\beta}\right) \quad (11)$$

$$Q(t) = H_u \cdot C_c \cdot \left(\frac{\tau}{t_e}\right)^{\beta} \cdot \left(\frac{\beta}{t_e}\right) \cdot \alpha_u \cdot \exp\left(-\left[\frac{\tau}{t_e}\right]^{\beta}\right) \cdot \exp\left(\frac{E_a}{R}\left(\frac{1}{273 + T_r} - \frac{1}{273 + T}\right)\right) \cdot \left(\frac{1}{3600}\right) \quad (12)$$

where t_e is the concrete equivalent age at the reference temperature as shown in Eq. 12 (h), H_u is the total amount of heat generated at 100 % hydration (J/kg), C_c is the total amount of cementitious materials (kg/m^3), τ is the hydration time parameter (h), β is the hydration slope parameter, α_u is the ultimate degree of hydration, E_a is the activation energy (J/mol), R is the universal gas constant (J/mol/K), T_r is the reference temperature (°C), and T_a is the average temperature during the time interval. At this point the degree of hydration, concrete maturity, rate of heat generation, and the adiabatic temperature rise can be calculated. Figure 5 shows an example of the previous

Table 3 Default chemical admixture dosages assumed if selected but not specified

Chemical admixture	Default percent used if not specified	
LRWR	0.0029	% By mass of cementitious materials
MRWR	0.0032	% By mass of cementitious materials
WRRET	0.0035	% By mass of cementitious materials
NHRWR	0.0078	% By mass of cementitious materials
PCHRWR	0.0068	% By mass of cementitious materials
ACCL	0.013	% By mass of cementitious materials

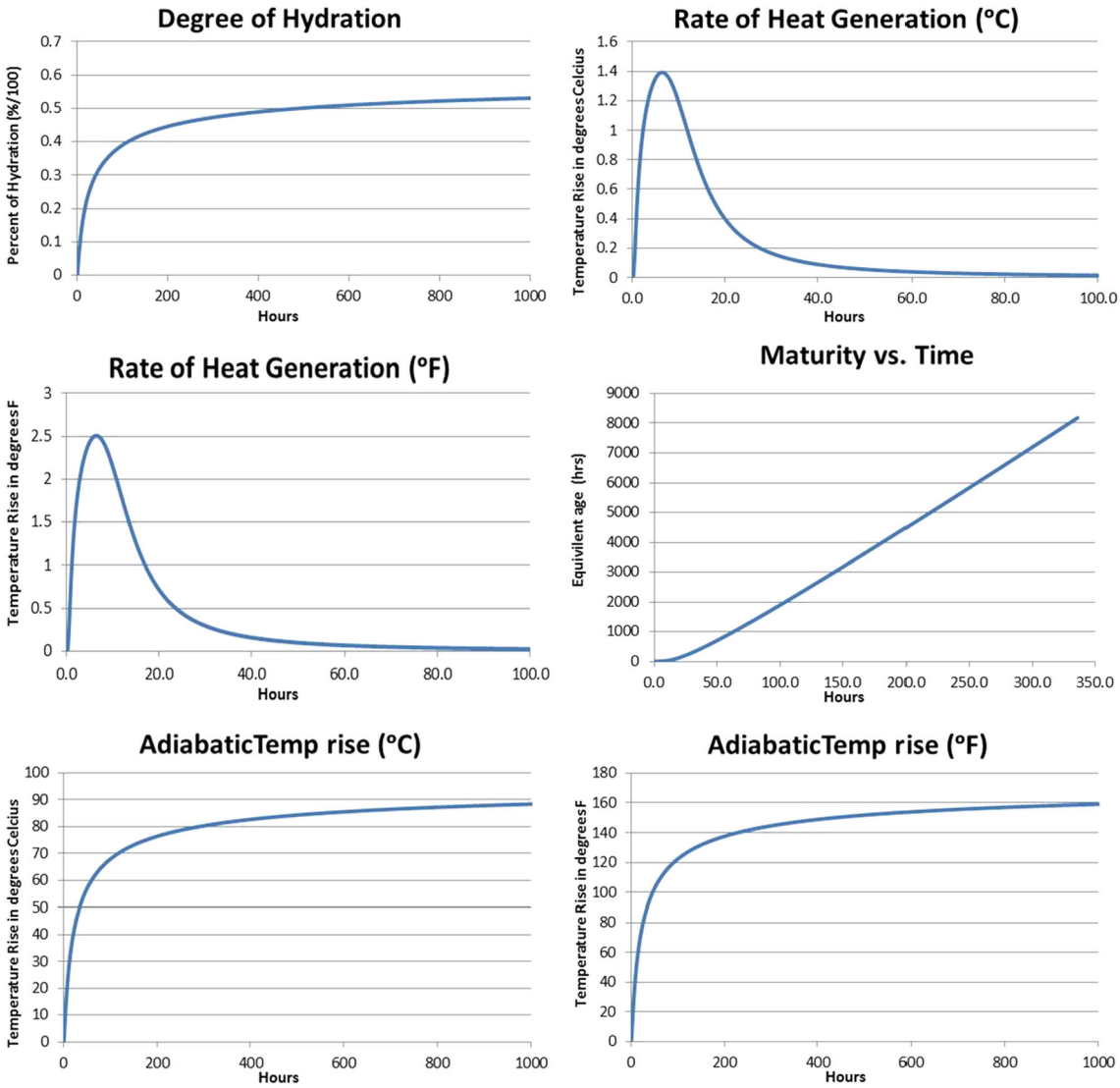

Fig. 5 Example of hydration properties

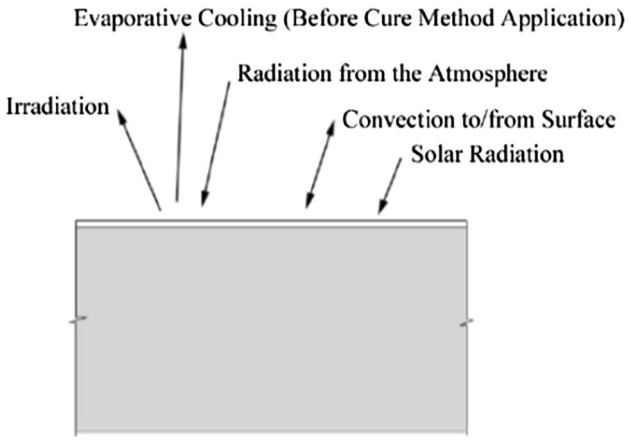

Fig. 6 Boundary conditions used for temperature analysis model

calculations which displays the graphs generated in this research.

Boundary conditions

The boundary conditions considered for the temperature analysis include many heat sources and sinks. The primary conditions models include: evaporative cooling, free and forced convection, conduction, atmospheric radiation, solar radiation and irradiation. A depiction of the boundary conditions modeled is shown in Fig. 6.

Evaporative cooling

The evaporative cooling model is from Schindler (2002). The model is reportedly based on the work of Menzel that

applied water evaporation rate equations developed by Koehler to concrete. The evaporation rate follows Dalton's law, which relates the water–vapor pressure of the air, at the water surface, and the wind speed to the evaporation rate (Hover 2006). Menzel's equation is shown as Eq. 13 (Al-Fadhala and Hover 2001).

$$E_w = 0.315(e_0 - RH \cdot e_a)(0.253 + 0.060w) \quad (13)$$

where E_w is the water evaporation rate (kg/m^2/h), e_0 is the water surface saturated water vapor pressure (mmHg), e_a is the air water vapor pressure (mmHg), RH is the relative humidity (as a decimal), and w is the wind speed (m/s). The amount of evaporation from concrete may be related to the amount of evaporation from a water surface by Eq. 14 (Schindler 2002):

$$E_c = E_w \cdot \exp\left[-\left(\frac{t}{a_{evap}}\right)^{1.5}\right] \quad (14)$$

where E_c is the evaporation rate from concrete (kg/m^2/h), t is the time from mixing (h), and a_{evap} is mixture-dependent time constant (h). The default value for a_{evap} is equal to 3.75 h, and the evaporative cooling model is applied until either a cure method is applied or 24 h after placing. The final change in heat due to evaporative cooling is calculated using Eq. 15.

$$\Delta Q = -E_c \cdot h_{lat} \quad (15)$$

where ΔQ is the heat lost due to evaporative cooling, E_c is the evaporation rate from the concrete as calculated in Eq. 14, and h_{lat} is calculated by using Eq. 16 where T_{sw} is the temperature of the surface water.

$$h_{lat} = 2,500,000 + 1859 \cdot T_{sw} \quad (16)$$

Convection

Both the free and forced convection heat exchanges are modeled using Eqs. 17 and 18. Equation 17 is defining the change in heat due to the convection process, and Eq. 18 is defining the convection coefficient.

$$\Delta Q = h(T_s - T_a) \quad (17)$$

$$h = C \cdot 0.2782 \cdot \left(\left[\frac{1}{T_{avg} + 17.8}\right]^{0.181}\right) \cdot \left(|T_s - T_a|^{0.266}\right) \cdot \left(\sqrt{1 + (2.8566 \cdot w)}\right) \quad (18)$$

where ΔQ is the change in heat, h is the convection coefficient, T_s is the temperature of the concrete surface, T_a is the temperature of the air, and T_{avg} is the average of the two temperatures.

Conduction

Conduction is the heat lost or gained from the contact of the concrete with any other material or substance. Conduction can be considered to act between the concrete and the air, between the concrete and the form work, or between the concrete and stagnate surface water; and is calculated using Eq. 19.

$$\Delta Q = -k \cdot A \cdot \frac{\Delta T}{\Delta y} \cdot \Delta t \quad (19)$$

where ΔQ is the change in heat, k is the thermal conductivity of the concrete, A is the area of contact, ΔT is the difference in temperature of the two materials, Δy is the thickness of the volume considered, and Δt is the duration of the time interval.

Radiation

The radiation that affects the curing concrete deck occurs as solar radiation, atmospheric radiation, and irradiation. The atmospheric radiation and irradiation are the easiest to calculate, and the respective equations are listed below in Eqs. 20 and 21.

$$\Delta Q = \sigma \cdot \varepsilon_a \cdot T_a^4 \quad (20)$$

$$\Delta Q = \varepsilon_c \cdot \sigma \cdot T_c^4 \quad (21)$$

where ΔQ is the change in heat due to the radiation, σ is the Boltzmann constant (W/m^{2}K^4), ε_a and ε_c are the emissivity values for either the air or the concrete, and T_a and T_c are the temperatures of either the air or the concrete. Solar radiations are much more complicated of calculations requiring calculated values for extraterrestrial radiation, solar declination angles, solar hour angles, and angles of incidence. These values are calculated based on the assigned latitude and longitude of the nearest location selected and follow the procedures outlined in "Solar Engineering of Thermal Processes: Third Edition" by J.A. Duffie and W.A. Beckman. However, the final equation used to calculate the solar radiation on the deck surface at any given time is defined in Eq. 22.

$$\Delta Q = (0.91 - 0.7 \cdot Cc) \cdot G_{on} \cdot Ab_c \quad (22)$$

where ΔQ is the change in heat due to solar radiation, Cc is the percent of cloud cover, G_{on} is the extraterrestrial radiation that would hit the surface, and Ab_c is the absorptiveness of the concrete. Using the values calculated for Eqs. 15, 17, 19, 20, 21, and 22, the final temperature of the concrete accounting for the energy lost or gained is ultimately compiled to generate a graph of temperature versus time. An example of the generated graphs is available in Fig. 7.

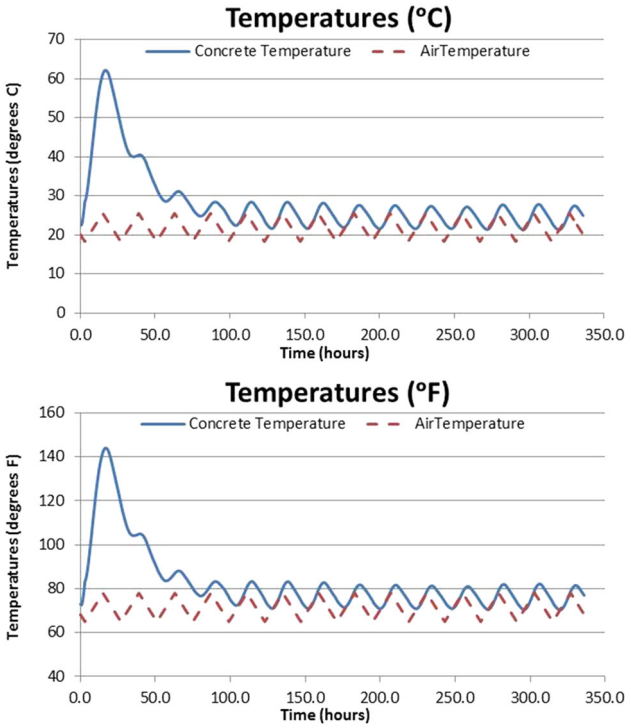

Fig. 7 Depiction of temperature analysis tab, displaying output graphs of temperatures

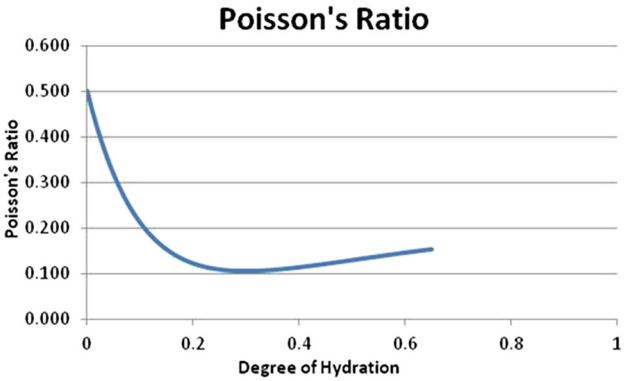

Fig. 8 Graphical depiction of example Poisson's ratio development

Thermal stress analysis

Thermal stress modeling in concrete members is nonlinear because of changing early-age material properties such as Poisson's ratio, the coefficient of thermal expansion (CTE), the modulus of elasticity, and the concrete strength. The nonlinearity is also attributed to differential temperature development and creep. The thermal stress analysis includes the evaluation of thermal expansion stresses, shrinkage stresses, the degrees of restraint, and the creep stresses developed over time. The B3 model associated with Zdenek P. Bazant and Sandeep Baweja was the primary source for the creep and shrinkage calculations where thermal, shrinkage, and creep strains are calculated and converted to stresses. The stresses are calculated from the strain values using Eq. 23.

$$\sigma = \frac{E_c \varepsilon}{(1+\nu)\cdot(1-2\nu)} \tag{23}$$

where σ is the developed stress, ε is the previously calculated strain, ν is the Poisson's ratio, and E_c is the modulus of elasticity of the concrete.

Concrete mechanical properties

Concrete mechanical property development at early ages is dependent on the concrete degree of hydration and temperature development. The mechanical property development is calculated using the equivalent age maturity (ASTM C 1074, 2004) as previously discussed.

(a) *Poisson's ratio*: A multitude of different equations have been developed to relate the maturity to the development of Poisson's ratio. This research uses a proposed model from Deschutter and Taerwe (1996); where Poisson's ratio is based on the degree of hydration as described in Eq. 24.

$$\nu(\alpha) = 0.18 \cdot \sin\left(\frac{\pi \cdot \alpha}{2}\right) + 0.5e^{-10\alpha} \tag{24}$$

where $\nu(\alpha)$ is Poisson's ratio at that degree of hydration and α is the degree of hydration as calculated from the heat of hydration analysis. An example of the graphical display of the Poisson's ratio used in this research is displayed in Fig. 8 (full hydration is not achieved in this example).

(b) *Coefficient of Thermal Expansion*: This research uses a constant CTE because of the lack of a data to model how the mixture proportions relate to CTE development. The constant coefficient of thermal expansion used is calculated from the mixture proportions and the aggregate type using the method proposed by Emanuel and Hulsey (1977) shown in Eq. 25.

$$\alpha_{cteh} = \frac{\alpha_{ca}\cdot V_{ca} + \alpha_{fa}\cdot V_{fa} + \alpha_p \cdot V_p}{V_{ca} + V_{fa} + V_p} \tag{25}$$

where α_{cteh} is the hardened concrete CTE, α_{ca} is the coarse aggregate CTE (με/°C), V_{ca} is the coarse aggregate volume (kg/m^3), α_{fa} is the fine aggregate CTE (με/°C), V_{fa} is the fine aggregate volume (kg/m^3), α_p is the paste CTE (με/°C), and V_p is the paste volume (kg/m^3). The default values of CTE for various constituents presented in Table 4 can be used for evaluation of the concrete's CTE in Eq. 25.

(c) *Compressive Strength*: The compressive strength of the concrete can be calculated in a number of ways. This research calculated the compressive strength of the concrete using two different methods and averages the results. The first method is described by Eq. 26.

Table 4 Default CTE values of concrete constituents used if no modifications are selected by user

Possible concrete constituents	Default CTE values used	
Hardened cement paste	10.8	μ ε/°C
Limestone aggregates	3.5	μ ε/°C
Siliceous river gravel and sands	11	μ ε/°C
Granite aggregates	7.5	μ ε/°C
Dolomitic limestone aggregates	7	μ ε/°C

$$f'c(t) = f'c_{28} \cdot \exp\left(-\left[\frac{\tau_s}{t}\right]^{\beta}\right) \tag{26}$$

where $f'c(t)$ is the concrete compressive strength at any given time t, $f'c_{28}$ is the concrete compressive strength at 28 days, τ_s is a fit parameter taken as 0.721, and β is another fit parameter taken as 27.8. In the other method, Eq. 27 is solved for $f'c(t)$ using the value from Eq. 28 as $E_c(t)$ and is averaged with the value attained from Eq. 26.

(d) *Modulus of Elasticity*: The elastic modulus provides the correlation between restrained strains and stresses, and it is known to be dependent on the mixture proportions, unit weight, maturity, aggregate modulus, strength, and moisture condition. The elastic modulus is also known to develop faster than the tensile and compressive strengths. In this research, two methods of calculating the modulus are performed and then averaged. The two methods are described by Eqs. 27 and 28 where Eq. 27 is from the ACI 318 document, and Eq. 28 is from the CEB-FIP document.

$$E_c(t) = 57,000\sqrt{f'c(t)} \tag{27}$$

$$E_c(t) = E_{c28}e^{\left[s/2\left(1-\sqrt{28/t}\right)\right]} \tag{28}$$

where $E_c(t)$ is the concrete modulus of elasticity at any time t, E_c28 is the concrete modulus of elasticity at 28 days, and s is a cement type coefficient which is 0.2 for high early strength cements, 0.25 for normal hardening cements, and 0.38 for slow hardening cements.

Thermal expansion

Thermal dilation stresses developed in the concrete are the easiest stresses to calculate using the B3 model. The thermal dilation strain is defined as listed in Eq. 29.

$$\varepsilon_T(t) = \alpha \cdot \Delta T(t) \tag{29}$$

where ε_T is the thermal strain developed at time t, α is the concrete CTE as calculated in Eq. 25, and $\Delta T(t)$ is the difference in temperature from the reference temperature at time t. The relating thermal stresses are then calculated using Eq. 23.

Shrinkage

Concrete early-age free shrinkage strains are dependent on the concrete degree of hydration and temperature development. The free shrinkage strain is composed of the concrete thermal strains, the autogenous strains, the drying shrinkage strains, and the plastic shrinkage strains. In the B3 model, the shrinkage is first estimated from the concrete strength and composition, Eq. 30.

$$\varepsilon_{sh}(t) = -\varepsilon_{sh\infty} \cdot k_h \cdot S(t) \tag{30}$$

where $\varepsilon_{sh}(t)$ is the mean shrinkage strain in the cross section, $\varepsilon_{sh\infty}$ is the time dependence of ultimate shrinkage, k_h is the humidity dependence, and $S(t)$ is the time dependence for shrinkage. These variables can easily be calculated using the B3 model.

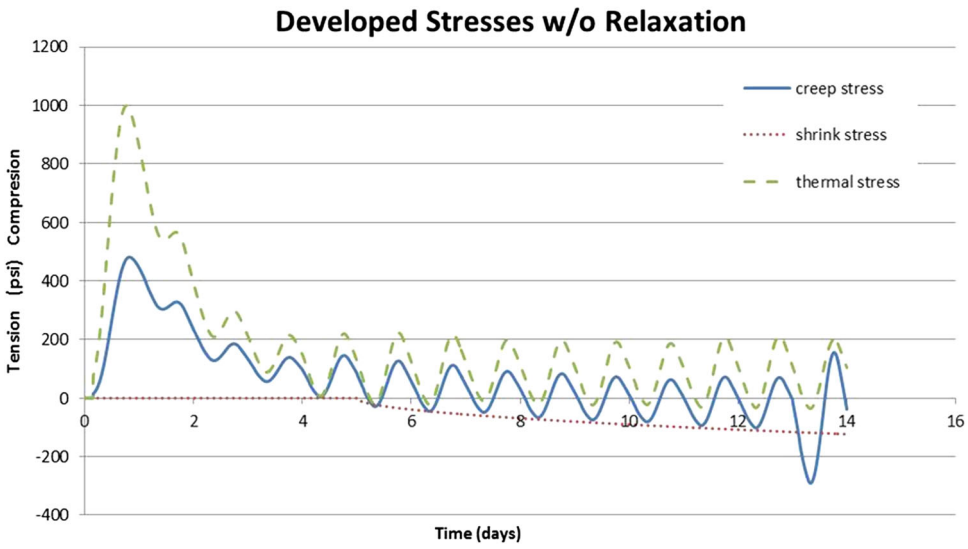

Fig. 9 Example of stresses w/o relaxation calculated

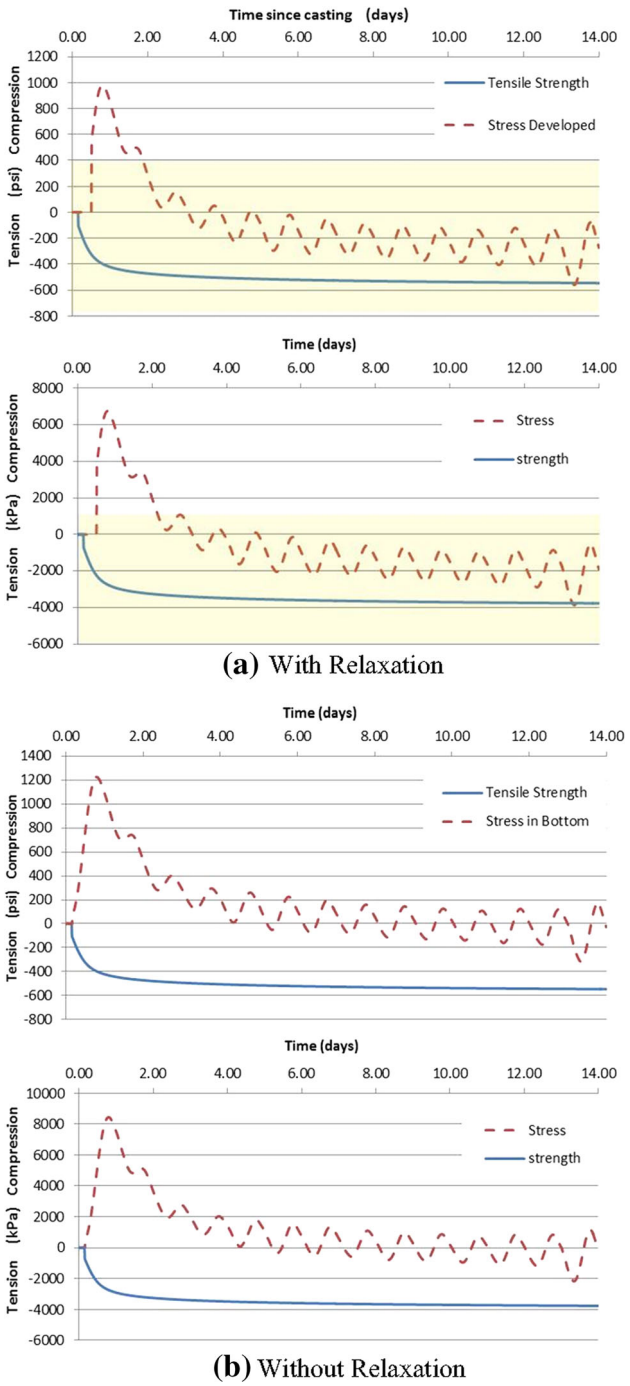

Fig. 10 Stresses and tensile strengths with time. **a** With relaxation, **b** without relaxation

Creep

The creep calculated in this research is primarily due to the applied stresses from early-age thermal stresses and shrinkage stresses prior to loading. The final equation for the calculation of the early-age creep strains is defined in Eq. 31.

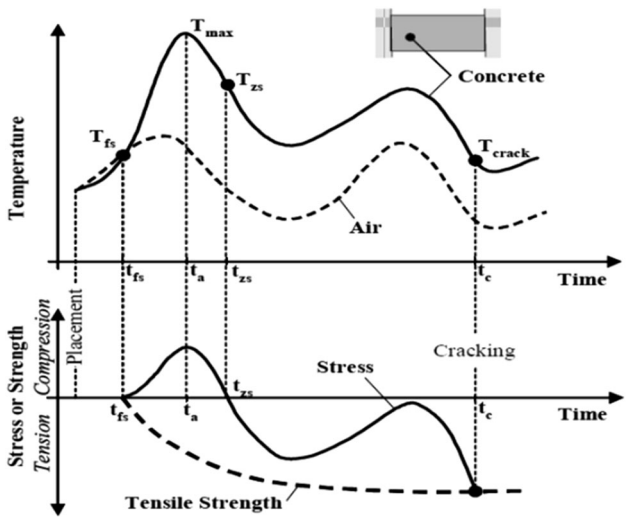

Fig. 11 Documented behavior of hardening concrete and crack identification (Schindler 2002)

$$\varepsilon_{cr}(t) = J(t) \cdot \sigma(t) \tag{31}$$

where $\varepsilon_{cr}(t)$ is the creep strain at any time t, $J(t)$ is the creep compliance function as described in Eq. 32, and $\sigma(t)$ is the stress in the concrete at any time t.

$$J(t) = q_1 + C_0(t) + C_d(t) \tag{32}$$

where $J(t)$ is as previously defined, q_1 is the instantaneous strain due to a unit stress, $C_0(t)$ is the compliance function for basic creep at any time t, and $C_d(t)$ is the compliance function for additional creep due to simultaneous drying. The aforementioned compliance functions can also be easily calculated following the B3 model for creep and shrinkage. An example of the developed stresses calculated is available in Fig. 9.

Tensile cracking prediction

Degrees of restraint

For the degree of restraint, the restraining materials modulus is defined as E_f, and the modulus of the freshly casted concrete is E_c. The ratio of the two moduli defines the degree of restraint as described in Eq. 33.

$$K_r = \begin{Bmatrix} 0.2 & \text{when} & \frac{E_f}{E_c} \le .1 \\ .33 & \text{when} & .1 < \frac{E_f}{E_c} \le .2 \\ .56 & \text{when} & .2 < \frac{E_f}{E_c} \le .5 \\ .71 & \text{when} & .5 < \frac{E_f}{E_c} \le 1 \\ .83 & \text{when} & 1 < \frac{E_f}{E_c} \end{Bmatrix} \tag{33}$$

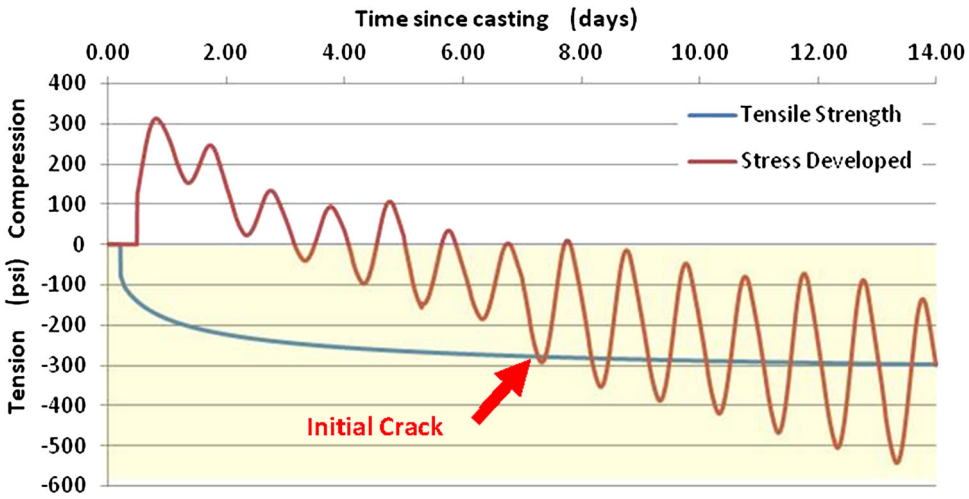

Fig. 12 Calculated behavior of hardening concrete sample and crack identification (Schindler et al. 2010)

Table 5 HIPERPAV versus deck cracking spreadsheet comparison summary

Case study (no—description)	HIPERPAV result (for concrete roadway pavement)	Deck cracking spreadsheet result (for reinforced concrete deck)
I—Cement type	Type III cement: requires saw cut before 12 h	Type III cement: cracks at 6 days
	Type I cement + fly ash: requires saw cut before 15 h	Type I cement + fly ash: cracks at 15 days
II—Aggregate type	Low CTE value: has wider crack spacing	Low CTE value: cracks at later time
	High CTE value: has narrower crack spacing	High CTE value: cracks at earlier time

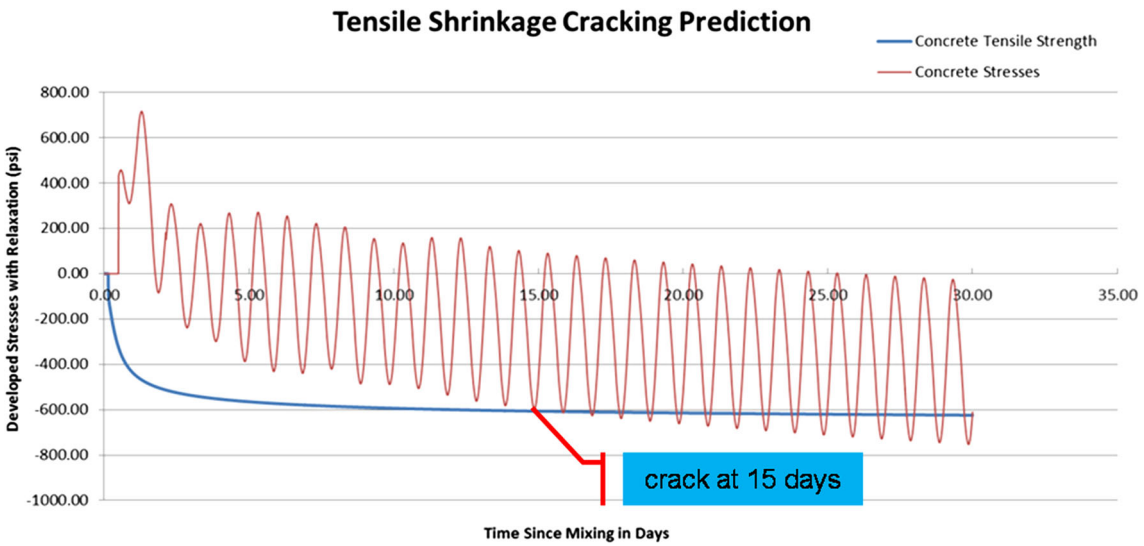

Fig. 13 Case study I: cement type I with fly ash

Total developed stresses

Using the stresses calculated from the strains in Eqs. 29, 30, and 31, the total stress in the newly casted deck can be calculated from Eq. 34.

$$\sigma_{\text{total}} = K_r \cdot (\sigma_J + \sigma_T + \sigma_{\text{cr}}) \tag{34}$$

Time of first developed crack

Finally, the tensile strength can be calculated by Eq. 35; where $f'c$ is as calculated in Eq. 26, and w is the calculated unit weight of the concrete determined from the mix design.

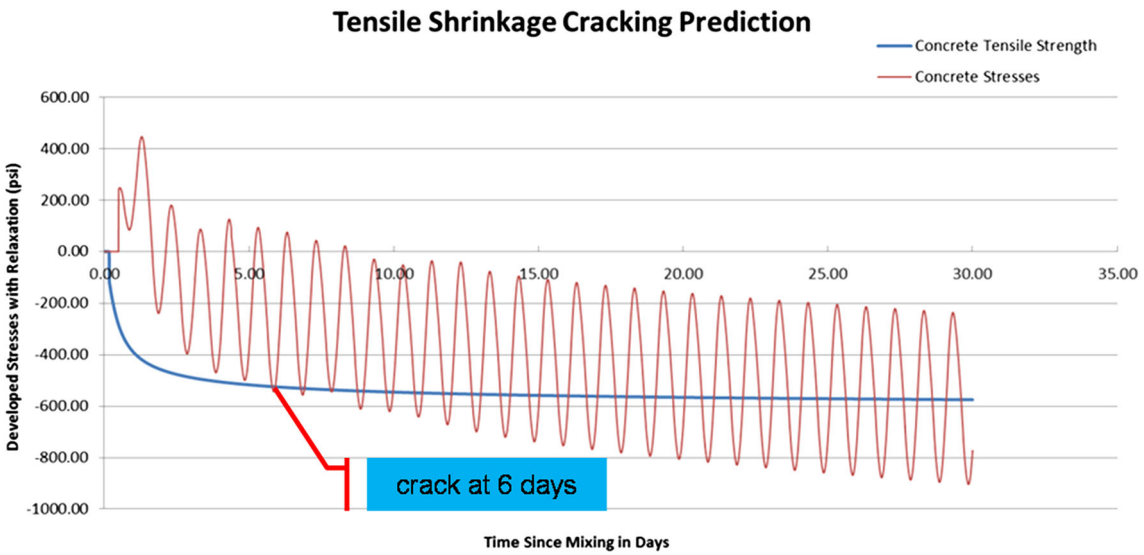

Fig. 14 Case study I: cement type III

$$f_t = \frac{\sqrt{f'c \cdot w}}{3} \tag{35}$$

The age of the concrete at initial cracking of the deck can be approximated by comparing the developed tensile strength of the concrete to the stresses developed in the concrete. An example of this comparison can be seen in Fig. 10.

Similar to the reference documents, when relaxation effects are taken into consideration, a point of zero stress can be identified, and the moment in time of cracking is shown by the first intersection of the two graphed properties (developed strength and developed stresses). An example of the theory is depicted in Fig. 11 which was taken from Schindler (2002). This research developed a graph which follows the concept in Fig. 11, and it is shown in Fig. 12 where the age of concrete at time of first cracking can be easily identified.

Comparison to HIPERPAV

The HIPERPAV® (*HI*gh *PER*formance Concrete *PAV*ing) software is used to analyze the early-age behavior of jointed concrete pavements, continuously reinforced concrete pavements, and bonded concrete overlays. It is important to compare results of developed spreadsheet to those of available tools, therefore, two HIPERPAV® case studies were run in the Deck Cracking Spreadsheet and the results were compared to results from HIPERPAV®. It was found that results have matched in most cases (Table 5).

Case study I

This HIPERPAV case study investigates how a change in cement type affects saw cutting and probability of cracking on a fast track project. Two concrete mix designs were analyzed, the first mix uses a Cement Type I with fly ash, and the second mix uses a Cement Type III. From results of HYPERPAV, it is anticipated that the mix using Type III Cement will develop cracks at an earlier age than the mix using Type I Cement with fly ash, and hence, the optimum time period for saw cutting may be reduced when Type III Cements are used. The results obtained from the Deck Cracking Spreadsheet, see Figs. 13 and 14, showed that concrete with Type I Cement and fly ash developed first crack at about 15 days, while concrete with Type III Cement developed first crack at about 6 days. It is clear that this finding agrees with performance observed when HYPERPAV was used.

Case study II

This HIPERPAV case study investigates how coarse aggregate type affects the performance of the CRCP for a set of climatic conditions. Five concrete mix designs were analyzed each with a different type of coarse aggregate. The Deck Cracking Spreadsheet is used to assess the behavior of an 11-inch CRCP constructed with concrete containing different aggregate types, namely siliceous river gravel (Lime), basalt, granite/gneiss, sandstone, and limestone. The climate is assumed to be for temperatures at noon on December 12. The contraction and expansion of the concrete deck depends on

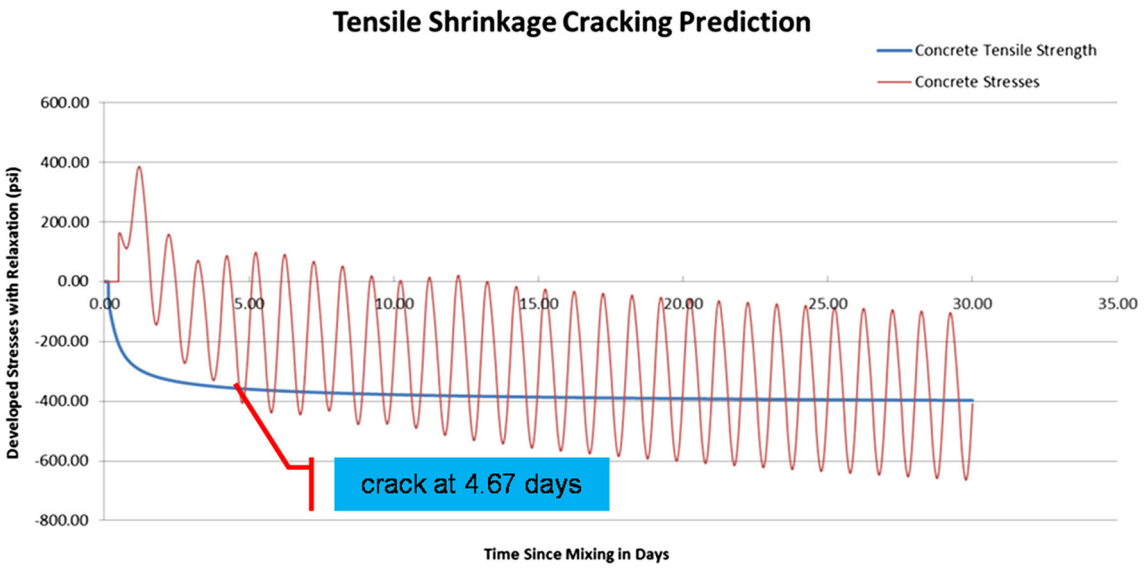

Fig. 15 Case study II: siliceous gravel

Table 6 Case study II: CTE results

Aggregate type	Limestone	Basalt	Granite	Sandstone	Siliceous gravel
CTE (με/°F)	2.6	3.7	4.2	6.2	6.5
Crack time (days)	23.76	4.69	8.75	4.69	4.67

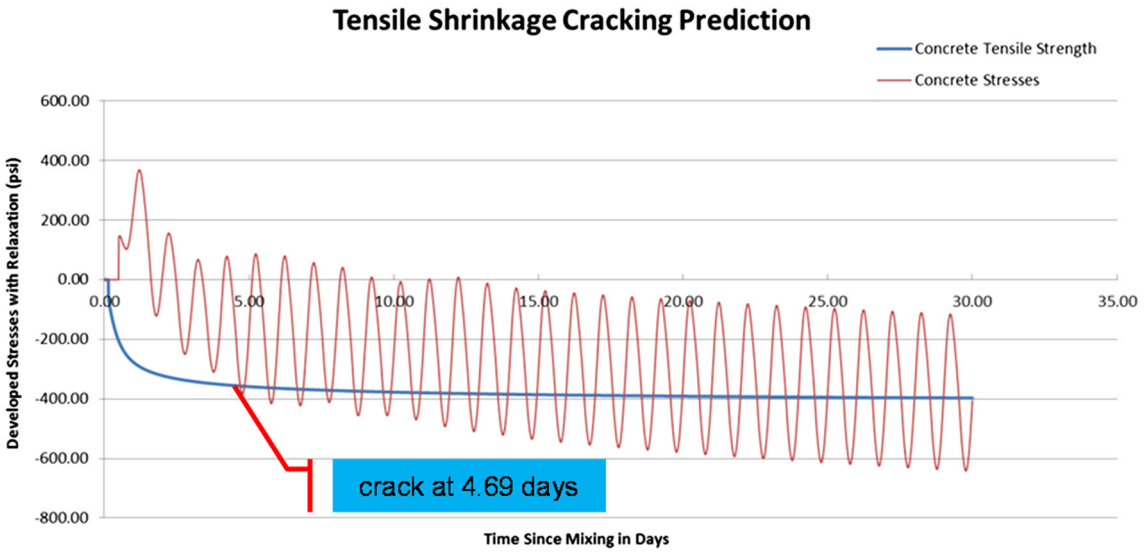

Fig. 16 Case study II: sandstone

the coarse aggregate coefficient of thermal expansion (CTE), since coarse aggregate comprises about half of the concrete volume. Since temperature changes are the greatest in the deck immediately after construction, its volume changes are significant at early ages. From the HIPERPAV results, it is anticipated that the pavement constructed with the low CTE aggregate provides better performance since it experiences lower thermal stresses. Results of spreadsheet for all the five cases (Fig. 15 through Fig. 19) are summarized in Table 6, and results show similar trend to those of HIPERPAV. With the exception of Basalt, which cracks at 4.7 days, all the other four types of coarse aggregates seem to follow the trend anticipated in the HIPERPAV models. The deck

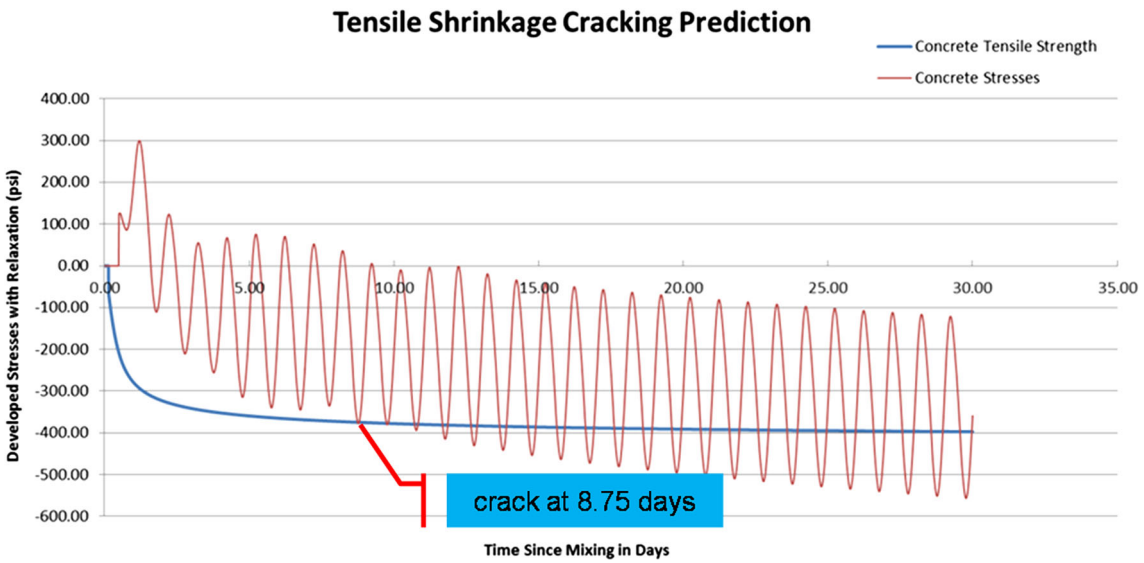

Fig. 17 Case study II: granite

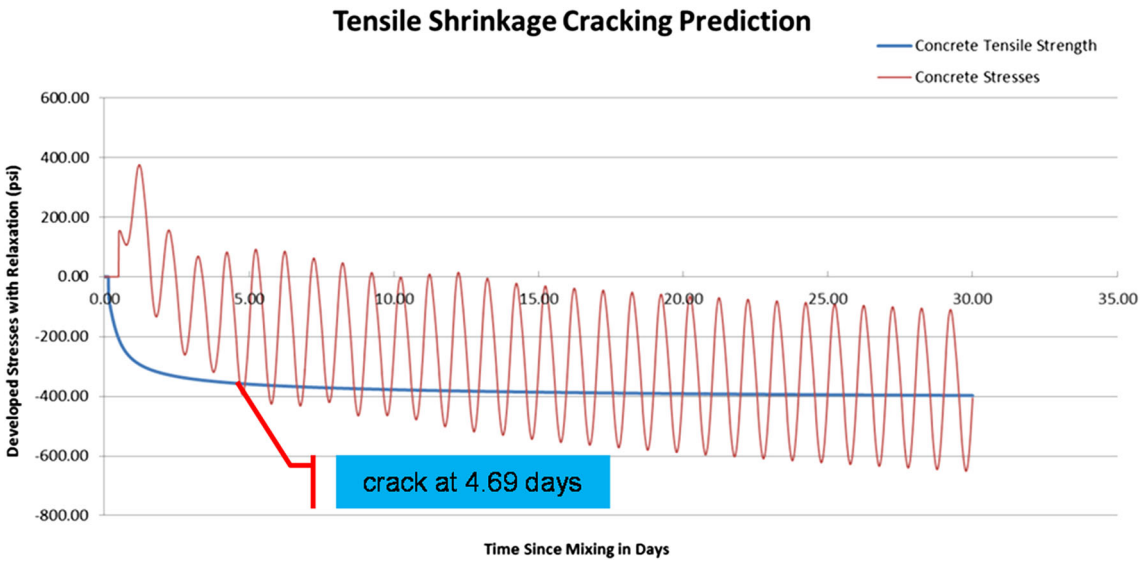

Fig. 18 Case study II: basalt

constructed with the low CTE aggregate provides better performance by cracking at a later time.

New deck analysis

The bridge under study consists of two simply-supported spans on AASHTO Type II beams. The deck is poured continuous over the intermediate bent.

The Deck and Concrete Input information is shown in Fig. 20. The project location is close to Lakeland Florida. Based on the design plans, the concrete deck is 8 inches thick, the 28 day compressive strength is 4500 psi. The top and bottom reinforcing steel mats consist of #5 rebars spaced at eight inches.

The Structure and Environmental information and input are shown in Fig. 21. Based on the progress reports obtained from CEI, it appears that the deck pour took place in the morning of June 11, 2012. The weather conditions for the first 14 days after the deck pour were obtained. The information includes the maximum and minimum temperatures, the maximum wind speed, and the maximum and minimum relative humidity.

The result summary is shown in Fig. 22. The graph theoretically shows that no cracks are anticipated to take

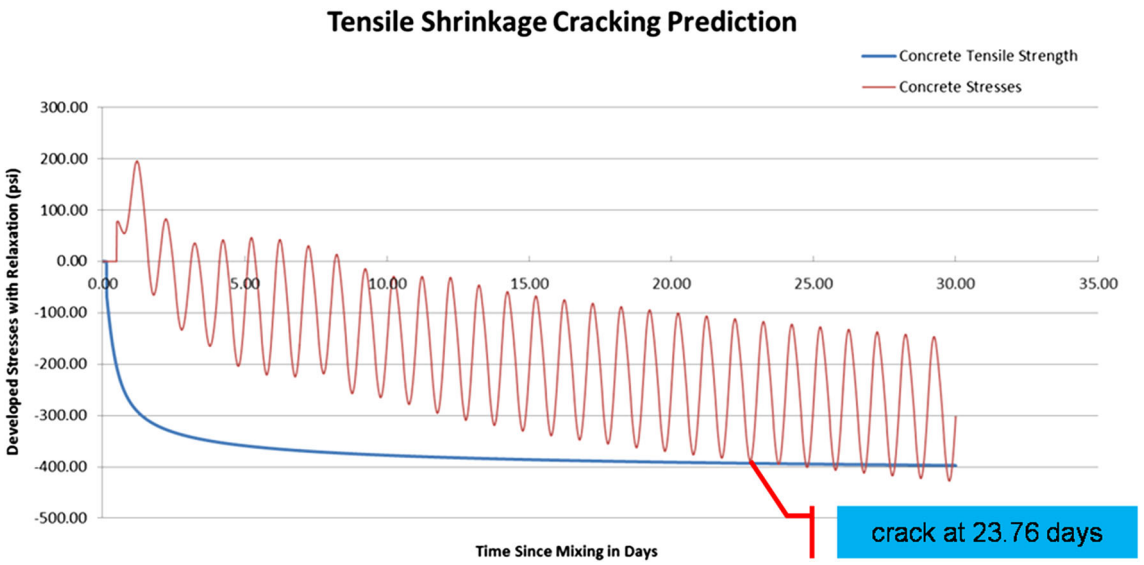

Fig. 19 Case study II: limestone

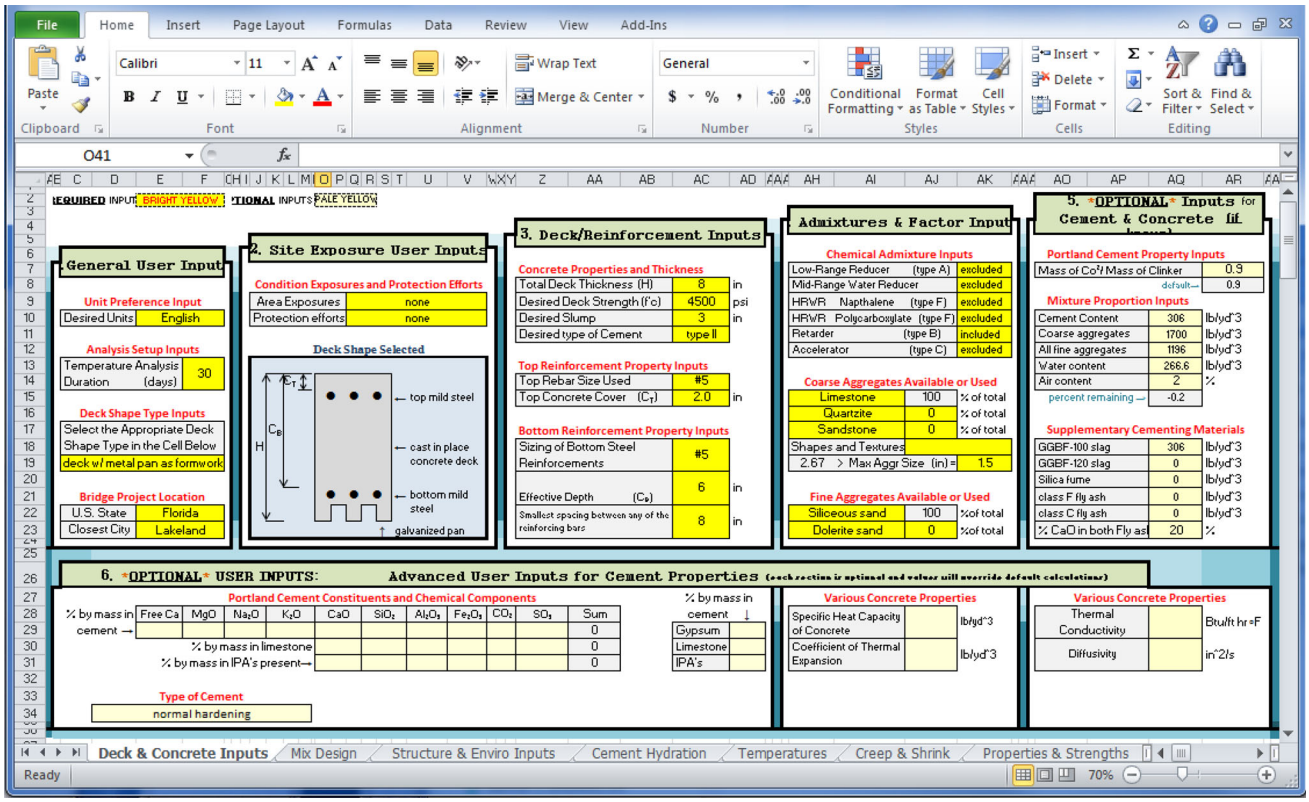

Fig. 20 New deck analysis: deck and concrete inputs

place in this new deck. This could be attributed to the following reasons:

1. The concrete mix design had taken into consideration hot weather concreting requirements.
2. The weather conditions seem to be favorable for deck pouring since the maximum relative humidity was over 95 % for 13 out of the 14 days after deck casting and the minimum relative humidity registered at 95 % on day 14.

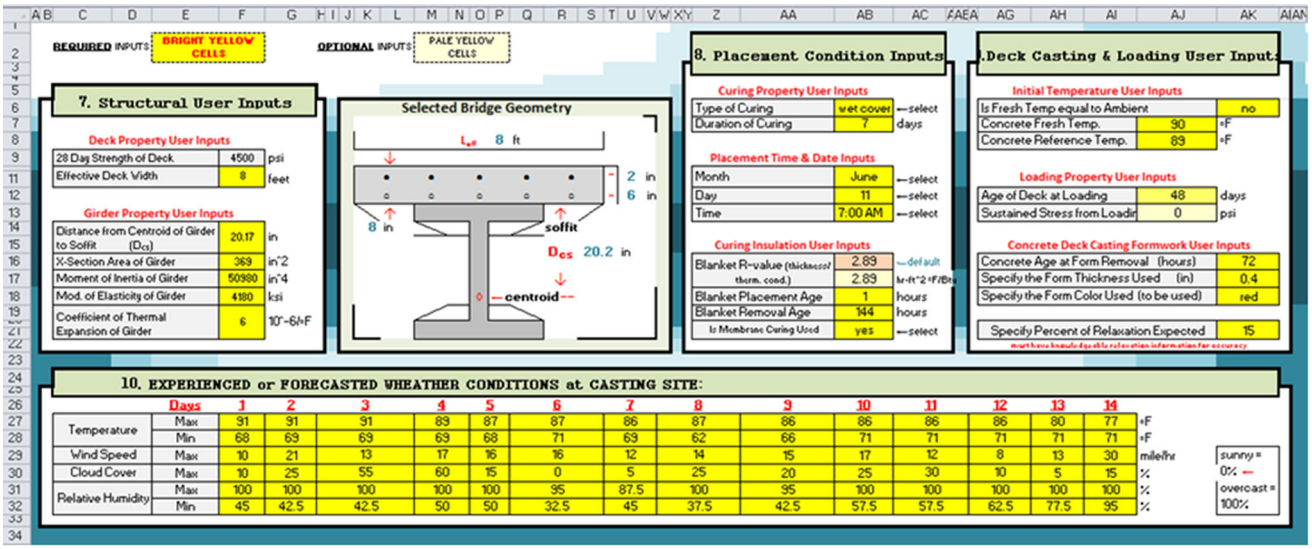

Fig. 21 New deck analysis: structure and environmental inputs

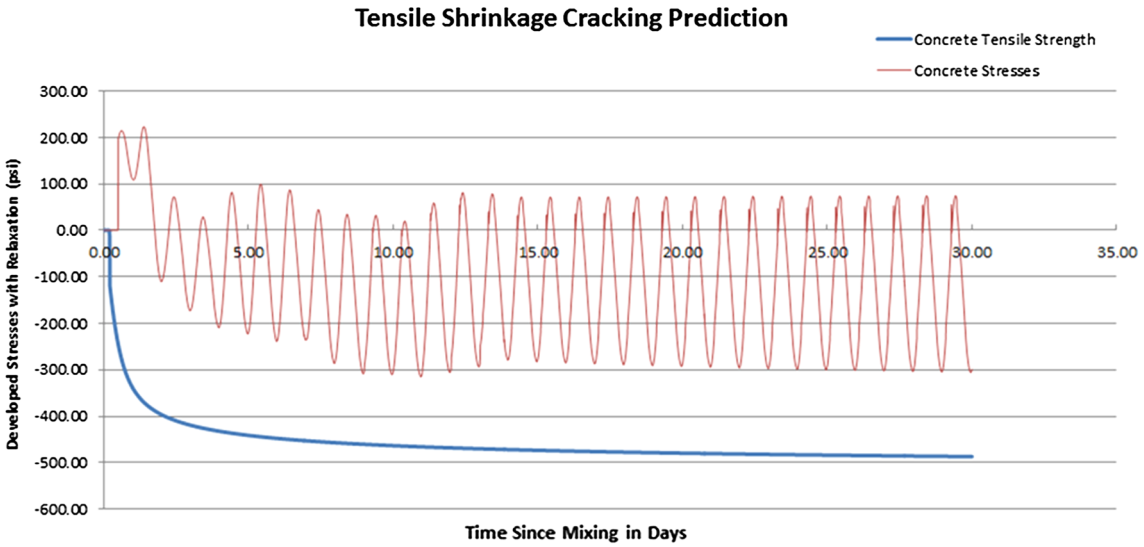

Fig. 22 New deck analysis: result summary

Conclusions

There are several conclusions drawn from this study including implementing a number of practical methods for evaluating and reducing the risk of early-age cracking such as reducing the placement temperature of the concrete, selecting an aggregate with a low coefficient of thermal expansion, using a favorable grading, using a large maximum size aggregate, using a relatively coarsely ground cement with a low alkali content, and a high sulfate content relative to its C_3A content, substituting some of the cement with fly ash, using entrained air, and using SRAs.

A tool was developed to predict transverse deck cracking based on the properties of the bridge deck, mix design, and environment and the types of loads applied. The availability of such tool is expected to make the evaluation of likelihood of cracking in bridge decks more efficient, since it displays both the developed stresses and when cracks may take place.

The Deck Cracking Spreadsheet is used for concrete bridge decks and addresses a few different types of construction including decks with stay-in-place galvanized forms, decks with removable forms, and decks on precast panels. The program can be accessed through FDOT. The Deck Cracking Spreadsheet is a user-friendly calculation tool for concrete mixture proportioning, temperature prediction, thermal analysis, and tensile cracking prediction. The Deck Cracking Spreadsheet results were also

compared with the HIPERPAV® software results by conducting a number of case studies.

Also, users can arrive at a crack-free design for bridge deck using the developed tool by inputting the concrete mix design, taking into consideration hot weather concreting requirements, and favorable weather conditions. The tool's graph theoretically can show that no cracks are anticipated to take place in this designed concrete bridge deck.

References

Al-Fadhala M, Hover KC (2001) Rapid evaporation from freshly cast concrete and the Gulf environment. Constr Build Mater 15(1):1–7

American Association of State Highway and Transportation Officials (AASHTO) (2007) LRFD bridge design specifications, 4th Edition, Washington DC

American Concrete Institute (2009) ACI Committee 211: "Standard practice for selecting proportions for normal, heavyweight and mass concrete". American Concrete Institute, Farmington Hills

American Concrete Institute (2010) ACI Committee 231, "report on early-age cracking: causes, measurement, and mitigation (ACI 231R–10)". American Concrete Institute, Farmington Hills, p 46

American Concrete Institute Committee 301, Specifications for Structural Concrete 2010

Babaei K, Hawkins NM (1987) Evaluation of bridge deck protective strategies. NCHRP report 297, TRB, National Research Council, Washington, DC

Babaei K, Purvis RL (1996) Premature cracking of concrete bridge decks: cause and methods of prevention. In: Proceedings, 4th international bridge engineering conference

Darwin D, Browning J, Mcleod HAK, Lindquist W, Yuan J (2012) Implementing lessons learned from twenty years of bridge-deck crack surveys. ACI Spec Publ 284:1–18

Deschutter G, Taerwe L (1996) Estimation of early-age thermal cracking tendency of massive concrete elements by means of equivalent thickness. ACI Mater J 93(5):403–408

El Safty A, Abdel-Mohti A, Jackson NM, Lasa I, Paredes M (2013) Limiting early-age cracking in concrete bridge decks. Adv Civil Eng Mater 2(1):379–399. doi:10.1520/ACEM20130073 **ISSN 2165-3984**

ElSafty A, Abdel-Mohti A (2013) Investigation of likelihood of cracking in reinforced concrete bridge decks. Int J Concr Struct Mater (IJCSM), 7(1):79–93

ElSafty A, Jackson NM (2012) Sealing of cracks on florida bridge decks with steel girders. Report, FDOT Contract #BDK82 977-02, FDOT, State Research Office, Tallahassee

Emanuel JH, Hulsey JL (1977) Prediction of the thermal coefficient of expansion of concrete. J Am Concr Inst 74(4):149–155

French C, Eppers L, Le Q, Hajjar JF (1999) Transverse cracking in concrete bridge decks. Transportation research record. n 1688, pp 21–29

Manafpour A, Hopper T, Radlinska A, Warn G, Rajabipour F, Morian D, Jahangirnejad S (2015) Bridge deck cracking: effects on in-service performance, prevention, and remediation. Pennsylvania Department of Transportation, Report

Hover KC (2006) Evaporation of water from concrete surfaces. ACI Mater J 103(5):384–389

Krauss PD, Rogalla EA (1996) Transverse cracking in newly constructed bridge decks. NCHRP Report 380, Transportation Research Board, Washington

La Fraugh RW, Perenchio WF (1989) Phase I report of bridge deck cracking study West Seattle Bridge. Report No 890716, Wiss, Janney, Elstner Associates, Northbrook, Ill

Maggenti R, Knapp C, Fereira S (2013) Controlling shrinkage cracking: available technologies can provide nearly crack-free concrete bridge decks. Concr Int 35(7):36–41

McLeod HAK, Darwin D, Browning J (2009) Development and construction of low-cracking high performance concrete (LC-HPC) bridge decks: construction methods, specifications, and resistance to chloride ion penetration. SM report 94. University of Kansas Center for Research, Lawrence

PCA (1970) Durability of concrete bridge decks. Final report, p 35

Peyton SW, Sanders CL, John EE, Hale WM (2012) Bridge deck cracking: a field study on concrete placement, curing, and performance. Constr Build Mater 34:70–76. doi:10.1016/j.conbuildmat.2012.02.065

Schindler AK (2002) Concrete hydration, temperature development, and setting at early-ages. Ph.D. Dissertation, The University of Texas at Austin, Texas

Schindler AK, Folliard KJ (2005) Heat of hydration models for cementitious materials. ACI Mater J 102(1):24–33

Schindler AK, Hughes ML, Barnes RW, Byard BE (2010) Evaluation of cracking of the US 331 bridge deck. Report No. FHWA/ALDOT 930-645, Highway Research Center, Auburn, AL, p 150

Schmitt TR, Darwin D (1999) Effect of material properties on cracking in bridge decks. J Bridge Eng ASCE 4(1):8–13

Slatnick S, Riding KA, Folliard KJ, Juenger MCG, Schindler A (2011) Evaluation of autogenous deformation of concrete at early ages. ACI Mater J 108(1):21–28

Van Breugel K (1998) Prediction of temperature development in hardening concrete. In: Springenschmid R, editor. Prevention of thermal cracking in concrete at early ages. E&FN Spon, London; pp 51–75. RILEM Report 15 [Chapter 4]

Wan B, Foley CM, Komp J (2010) Concrete cracking in new bridge decks and overlays. WHRP Report 10-05, Wisconsin Highway Research Program, p 154

Wright JR, Rajabipour F, Laman JA, Radlińska A (2014) Causes of early age cracking on concrete bridge deck expansion joint repair sections. Adv Civil Eng 2014:10. doi:10.1155/2014/103421

Florida Department of Transportation Standard Specifications for Road and Bridge Construction

Florida Department of Transportation Structures Manual Volume 1 Structures Design Guidelines

Ohio Department of Transportation Bridge Design Manual

Pennsylvania Department of Transportation Design Manual Part 4 Structures (DM-4)